Jurnal Teknologi

Full Paper

DISTRIBUTION ANALYSIS OF MICRO-EARTHQUAKES IN GEOTHERMAL AREAS BY USING COUPLED VELOCITY-HYPOCENTER AND DOUBLE DIFFERENCE METHODS

Widya Utama[a]*, Sherly Ardhya Garini[b], Rista Fitri Indriani[c]

[a]Department of Geophysical Engineering, Institut Teknologi Sepuluh Nopember, 60111, Surabaya, Indonesia
[b]Department of Informatics, Institut Teknologi Sepuluh Nopember, 60111, Surabaya, Indonesia
[c]Department of Geomatics Engineering, Institut Teknologi Sepuluh Nopember, 60111, Surabaya, Indonesia

Article history
Received
20 March 2022
Received in revised form
13 October 2025
Accepted
14 October 2025
Published Online
30 April 2026

*Corresponding author
widya@geofisika.its.ac.id

Graphical abstract

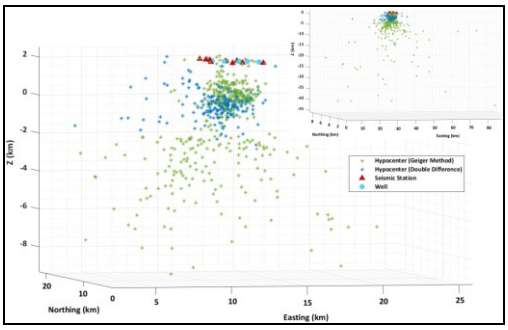

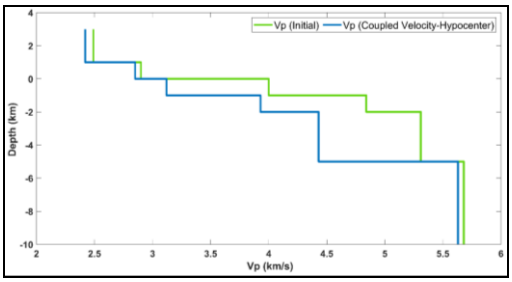

Abstract

Accurate and unbiased determination of hypocenter locations remains a major challenge in microearthquake (MEQ) studies. The reliability of the determination process greatly contributes to the real-time monitoring of geothermal reservoir activities. Therefore, this study focuses on monitoring geothermal reservoirs through the spatial distribution of MEQ locations using inversion methods. The inversion methods applied in this research include the single hypocenter determination method, which is used to identify the initial locations of MEQs, and the Coupled Velocity-Hypocenter simultaneous inversion method, which is employed to derive a new 1D velocity model for the MEQ cluster area. In addition, the Double-Difference method is utilized to enhance the accuracy of MEQ hypocenter locations by considering coherence factors between hypocenters. The data processing workflow demonstrates that the 1D velocity model refined by incorporating station corrections within the MEQ cluster area significantly improves the accuracy of hypocenter locations in the geothermal zone. This improvement is evidenced by a reduction of the average RMS residual to 0.07 s, indicating that the relocated hypocenters are reliable and that the derived velocity structure effectively represents the subsurface and approximates the true seismic velocity distribution. Most relocated MEQs are concentrated around the injection and production well zones, with approximately 94.3% of events occurring between 0.5 and -1.5 km depth, corresponding to the active geothermal reservoir. These clusters delineate fracture zones characterized by intense fluid flow activity.

Keywords: Coupled velocity-hypocenter, double-difference relocation, geothermal, hypocenter determination, micro-earthquake (MEQ)

1.0 INTRODUCTION

The development of geothermal systems involves continuous fluid extraction and injection that progressively modify the physical and mechanical properties of reservoir rocks [1]–[3]. Previous studies (e.g., Maurer *et al*., 2020) have shown that fluid circulation and pressure variations alter the stress field, enhance anisotropy, and trigger fracture activation [4]. These processes affect subsurface conditions by changing pore pressure, stress distribution, and fluid volume, leading to fracture formation or reactivation expressed as clusters of microearthquakes (MEQs) [5], [6]. Consequently, the spatial and temporal distribution of MEQs provides essential insights into reservoir dynamics and fluid migration within geothermal fields [7]–[9].

Accurate MEQ hypocenter determination is crucial for evaluating reservoir performance and operational safety [10]–[13]. owever, precision is often constrained by phase-picking errors, limited station geometry, and velocity-model bias. Previous studies highlight that refining network configuration and velocity models significantly improves depth accuracy and reduces hypocentral errors [14], [15].

This study was conducted in a vapor-dominated geothermal field located in East Java, Indonesia, characterized by active fault zones and high subsurface fluid circulation. Seismic monitoring was carried out using eleven broadband seismometers deployed around the production and injection well clusters. Each station operated at a sampling rate of 100 samples per second, with a frequency response of 0.1–50 Hz [16]–[20]. These settings ensured sufficient temporal resolution and signal fidelity for detecting low-magnitude events typical of geothermal environments [21], [22]. After signal-to-noise (S/N) evaluation and precise P-S phase picking, a sequential inversion workflow was implemented to improve spatial accuracy. The Geiger method was first applied to determine initial hypocenters, followed by Coupled Velocity-Hypocenter inversion to refine the 1D P-wave velocity model [15], [23], [24]. Final relocation using the Double-Difference method minimized differential travel-time residuals between closely spaced events. Simultaneously, the Vp/Vs ratio derived from the Wadati diagram was used to assess lithological variations and fluid saturation within the reservoir [14], [25]. This integrated approach effectively reduces velocity-model bias and enhances MEQ location accuracy, providing a robust basis for interpreting fracture connectivity and reservoir dynamics in geothermal systems [9], [20].

2.0 METHODOLOGY

The distribution of micro-earthquake (MEQ) hypocenters was determined through an inversion workflow designed to maximize spatial accuracy and minimize residual errors [26]. The precision of these results primarily depends on the quality of seismic recordings, the accuracy of P and S wave picking, the network geometry, and the appropriateness of the velocity model [27]. As highlighted by Leong and Zhu (2024), iterative location algorithms achieve optimal solutions by minimizing the misfit between observed and calculated travel times, while Blanck *et al*. (2022) demonstrated that double-difference relocation combined with waveform cross-correlation can substantially enhance event precision [28], [29]. Building on these principles, this study applies an integrated stepwise procedure to ensure reliable and high-resolution mapping of MEQ activity within the geothermal field [30].

2.1 Waveform Processing and Phase Picking

Waveform data were recorded by eleven broadband seismometers operating at 100 samples per second. The P and S wave arrivals were manually identified using Seisgram2K, which enables precise visualization of amplitude and frequency variations. After applying a strict quality-control threshold, 1,092 reliable phase arrivals were obtained [16]–[19]. Accurate phase picking is critical for hypocenter determination, as emphasized by Pei *et al*. (2025), who demonstrated that consistent manual identification achieves up to 98 % agreement with reference datasets [31]. Li *et al*. (2020) noted that waveform fidelity particularly sampling rate and instrument sensitivity directly affects inversion stability, while Zheng *et al*. (2025) and Dahal *et al*. (2024) highlighted that noise suppression and full-waveform analysis substantially reduce timing uncertainty [32]–[34]. Accordingly, this study applies rigorous waveform processing and manual phase picking to ensure the precision and reproducibility of seismic inversion results. The determination of P and S wave arrivals across all stations is shown in Figure 1.

2.2 Wadati Diagram and Geological Consistency

A Wadati diagram constructed from manually picked P and S wave arrivals yielded a Vp/Vs ratio of 1.12, indicating a stable velocity structure characteristic of steam saturated fractures in vapor dominated geothermal systems [35]. Similar findings were reported by Muttaqy *et al*. (2023) in Central and East Java and by Afnimar *et al*. (2015) beneath the Lembang Fault, both identifying low Vp/Vs values in fluid-rich volcanic deposits. The agreement with these studies supports the interpretation that the low Vp/Vs ratio observed here accurately represents steam-bearing fractured zones within the geothermal reservoir [25], [36]. The resulting Wadati diagram demonstrating this consistency is shown in Figure 2.

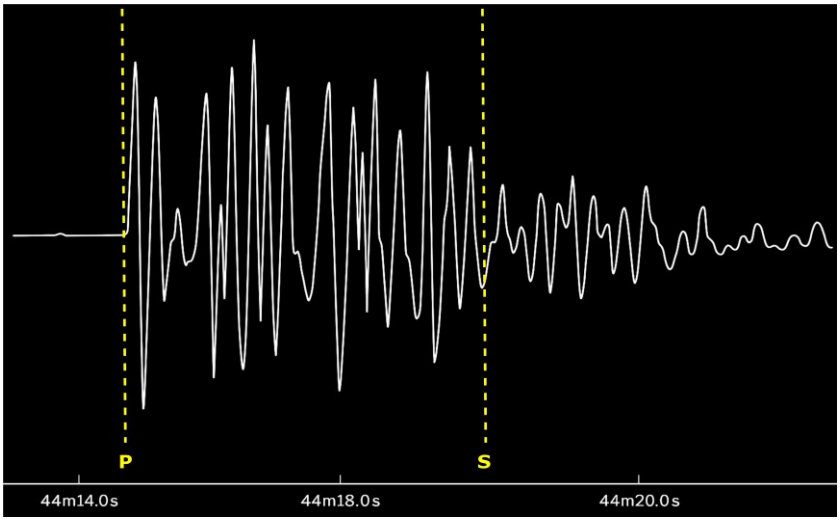

Figure 1 Determination of P and S wave arrival times

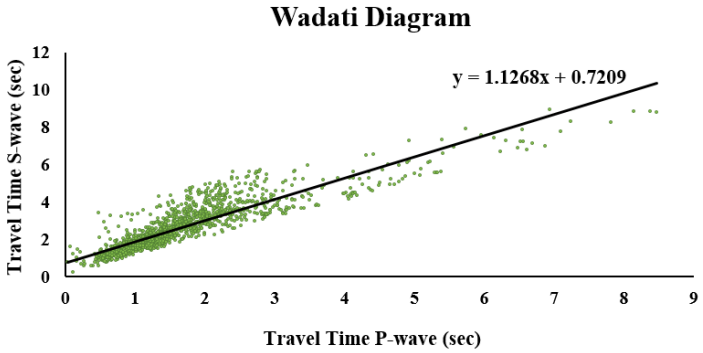

Figure 2 Wadati Diagram for the the selection of events to be consistent with geological information [25], [36]

2.3 Initial Hypocenter Estimation Using the Geiger Method

The initial MEQ hypocenters were estimated using the Geiger method, an iterative least-squares inversion that minimizes the residuals between observed and calculated P- and S-wave travel times. This classical single event approach employs station coordinates and a one dimensional velocity model to derive source positions and origin times [37]. As highlighted by Cheng *et al*. (2018) and Liao *et al*. (2022), the method remains a fundamental tool for earthquake and microseismic localization, efficiently linearizing the nonlinear source-location problem through successive iterations . Despite its sensitivity to phase-picking errors and simplified velocity assumptions, it provides a robust first-order approximation of hypocenter geometry [38], [39]. As noted by Wu *et al*. (2018), such initial estimates form the essential foundation for subsequent velocity-model refinement and event relocation [40].

2.4 Coupled Velocity–Hypocenter Inversion for 1-D Velocity Model Refinement

To improve event location accuracy, a coupled velocity-hypocenter inversion was performed using MATLAB based routines. This method simultaneously refines the one-dimensional velocity structure, hypocenter coordinates, and station corrections by minimizing travel-time residuals. The inversion utilized initial parameters from the Geiger results, P-S travel times, station coordinates, and the Vp/Vs ratio derived from the Wadati diagram, iterating until the RMS residual fell below 0.10 s with at least eight high-quality phases per event [9]. Previous studies Huang *et al*., (2019) have shown that joint inversion effectively reduces location bias caused by velocity heterogeneity, enhances the representation of layered structures, and improves microseismic mapping precision in geothermal reservoirs [41]. Consistent with these findings, the coupled inversion applied in this study significantly enhances both the reliability of the velocity model and the spatial accuracy of MEQ hypocenter determinations [42].

2.5 Double-Difference Relocation

Final hypocenter relocation was carried out using the Double-Difference algorithm in MATLAB to enhance spatial accuracy. The method minimizes differential travel-time residuals between pairs of nearby events recorded at common stations, assuming that closely spaced earthquakes share similar raypaths. This

approach effectively reduces common-mode errors caused by unmodeled velocity heterogeneity and yields precise relative locations. The processing used MAXDIST ≤ 15 km, MAXNGH ≤ 10, MINLINK = 8, and achieved an average RMS residual of 0.07 s [43]. Similar to findings by Muttaqy *et al*. (2023) in Central and East Java and by McBrearty and Beroza (2025), the use of waveform cross-correlation and differential times improves clustering consistency and fault delineation while minimizing depth uncertainty. Accordingly, the HypoDD method in this study provides a robust refinement of MEQ hypocenter distributions, ensuring reliable spatial patterns for subsequent geological and geothermal interpretation [14], [25].

2.6 Software Utilized

All inversion and relocation analyses were conducted using MATLAB based routines, providing a flexible and reproducible framework. MATLAB enables precise control of inversion parameters and ensures numerical stability throughout the processing workflow [44]. Lomax and Savvaidis (2022) highlighted its effectiveness for both probabilistic and deterministic earthquake localization [45]. Waveform visualization and phase picking were performed using *Seisgram2K*, which supports high-resolution inspection and interactive identification of P and S wave arrivals [46].

3.0 RESULTS AND ANALYSIS

Each stage, from waveform processing to final hypocenter relocation, was designed to enhance spatial resolution and minimize residual errors. Key metrics such as RMS residuals, depth distribution, and spatial clustering confirm the improved accuracy and reliability of the relocated hypocenters.

3.1 1-D Velocity Model Refinement

The one-dimensional (1-D) P-wave velocity model was refined using the Coupled Velocity-Hypocenter inversion, which simultaneously updates velocity parameters and event locations to minimize travel-time misfits. This approach was applied to the clustered MEQ dataset with station corrections to account for near-surface heterogeneity [47]. Figure 3 illustrates that while both initial and refined models share similar shallow gradients down to 2.3 km, notable improvements appear between 2.3 and 10 km, where the refined model yields smoother velocity transitions and enhanced vertical resolution. The P-wave velocity increases from 3.0 km/s near the surface to 5.5 km/s at depth, representing the transition from volcanic deposits to consolidated basement rocks [48]. The updated model, adopted for subsequent HypoDD relocation, substantially reduced RMS residuals and improved hypocenter clustering, thereby enhancing the structural interpretation of fault and fluid-related seismicity. Comparable studies by Huang *et al*. (2019), Okamoto *et al*. (2018), and Katsumata & Nishimiya (2025) similarly demonstrate that coupled inversion and refined local velocity structures significantly improve the accuracy of microseismic imaging in geothermal fields [42], [49].

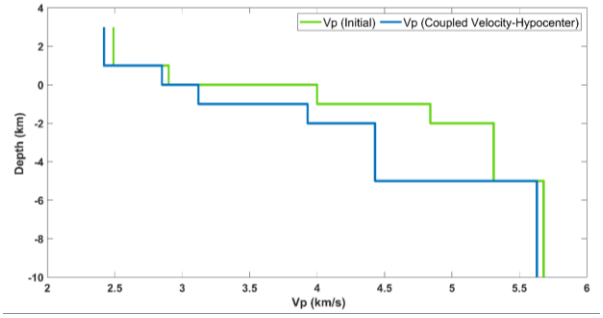

Figure 3 The comparison between the final 1D velocity model for the cluster area, obtained by Coupled Velocity-Hypocenter method with the initial velocity mode

3.2 Initial MEQ Hypocenter (Geiger Method)

The initial micro-earthquake (MEQ) hypocenters were determined using the classical Geiger travel-time inversion method applied to three months of continuous seismic data from eleven broadband stations within the geothermal field. A total of 457 events were successfully located, with 88.84 % situated within the survey boundary and 11.16 % outside due to edge-array limitations. The RMS residuals ranged from 0.01 s to 38.97 s (average 0.86 s), consistent with the sensitivity of the Geiger algorithm to arrival-time and velocity-model uncertainties as noted by Cheng *et al*. (2018) [38]. The resulting epicenters (Figures 4-6) show broad spatial dispersion around production and injection wells, with only partial alignment to mapped fault traces—a pattern commonly produced by irregular station geometry [39]. Hypocentral depths vary from -41.1 km to +2.3 km, with 37.1 % of events concentrated between -0.5 km and +0.5 km, corresponding to the upper geothermal reservoir. This vertical spread reflects uncorrected velocity heterogeneity, a known limitation of conventional Geiger localization, whereas the shallow clustering indicates active microseismicity within thermally and hydraulically influenced zones. Collectively, these preliminary results form a first-order baseline for subsequent Double-Difference relocation and velocity refinement.

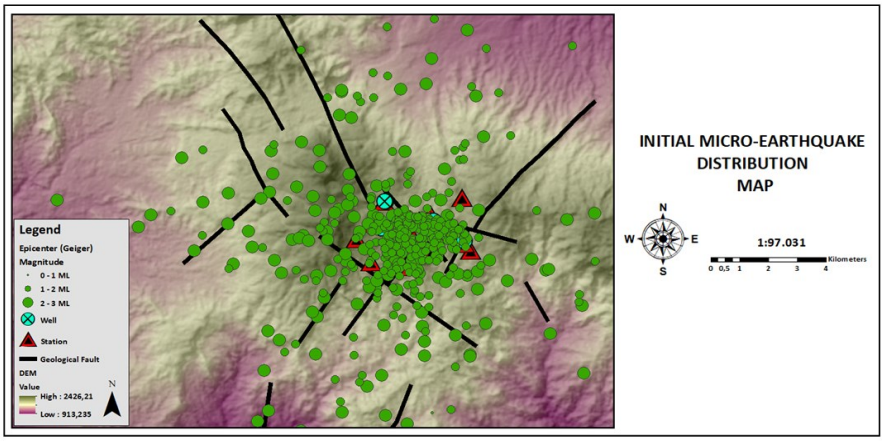

Figure 4 The distribution map of initial MEQ epicenter location as a result of Geiger method

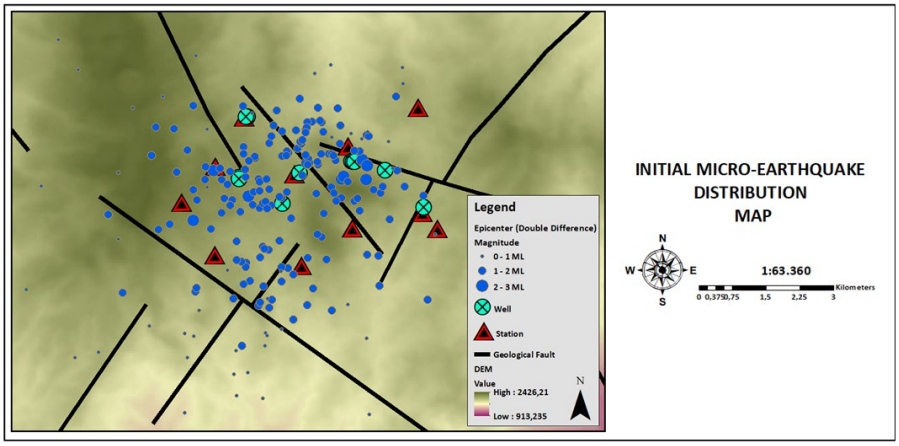

Figure 5 Zoomed-in area in figure 4, the whole location of MEQ epicenter location as a result of Geiger method

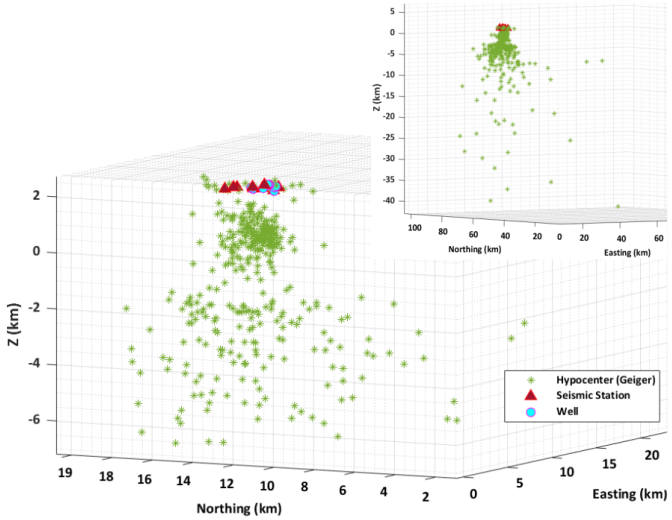

Figure 6 The distribution of initial MEQ hypocenter based on Geiger method, represented by the green dots

3.3 Relocated MEQ Hypocenter (Double-Difference Method)

The relocation of micro-earthquake (MEQ) hypocenters was conducted using the Double-Difference (HypoDD) algorithm with the refined 1-D velocity model derived from the previous inversion stage. Optimized parameters MAXDIST ≤ 15 km, MAXNGH ≤ 10, MINLINK = 8, and RMS residual 0.07 s, were applied to minimize travel-time bias and ensure stable convergence [43]. As noted by Muttaqy *et al.* (2023), these configurations enhance relative

accuracy by correlating residuals among neighboring events that share similar raypaths. The relocated epicenters (Figures 7-9) display tighter clustering and improved spatial coherence compared to the Geiger results, with most events concentrated near production and injection wells, reflecting fluid-induced seismicity within the geothermal reservoir. Peripheral clusters along mapped fault traces indicate fracture reactivation, consistent with regional microseismic patterns in East Java volcanic fields [25]. Vertically, the hypocenters range from -2.6 km to +2.1 km, with 94.3% of events confined between -1.5 km and +0.5 km, marking the reservoir zone. The 93.66% reduction in vertical scatter confirms the enhanced precision achieved through HypoDD relocation, in agreement with the findings of McBrearty and Beroza (2025), who demonstrated the method's capability to suppress common-mode velocity errors and refine focal-depth accuracy [14].

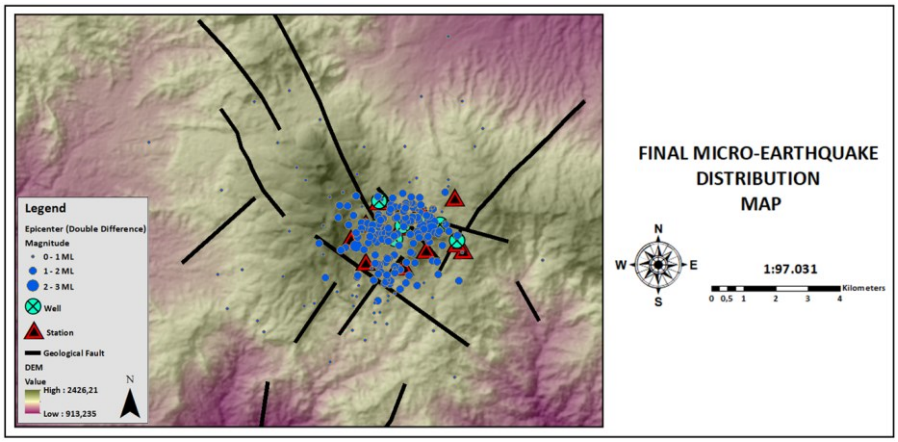

Figure 7 The distribution map of MEQ epicenter location as a result of Double-Difference method

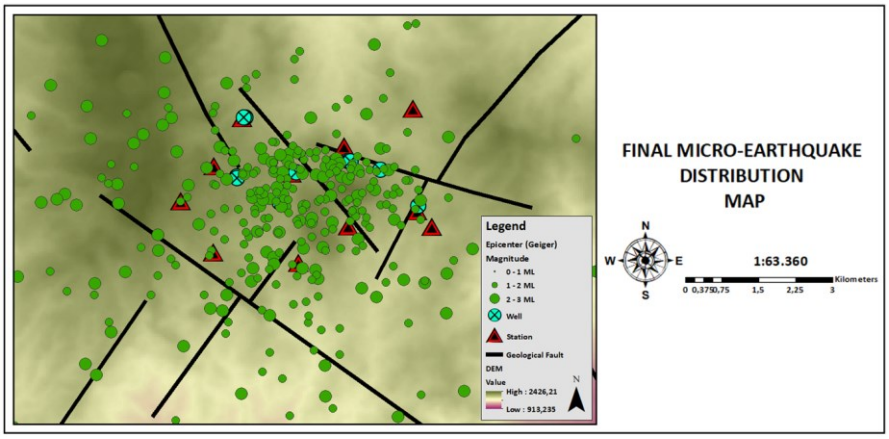

Figure 8 Zoomed-in area in figure 7, the whole location of MEQ epicenter location as a result of Double-Difference method

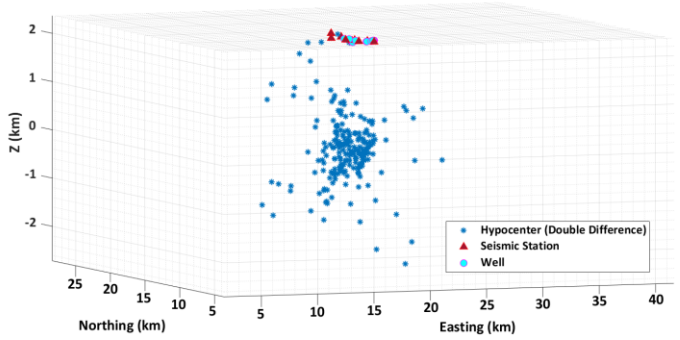

Figure 9 The distribution of MEQ hypocenter from Double-Difference method, represented by the blue dots

3.4 Quality Metrics and RMS Residual Comparison

The reliability of the relocated micro-earthquake (MEQ) hypocenters was assessed using Root Mean Square (RMS) residuals as the primary quality indicator. The comparison between the initial Geiger and the final Double-Difference (HypoDD) solutions (Figure 10) shows a substantial improvement, with RMS values reduced from a wide 0.01–38.97 s range to a narrow 0.00-0.09 s interval (average of 0.07 s). Over 90% of relocated events exhibit RMS ≤ 0.1 s, confirming strong agreement between observed and calculated arrivals and significantly enhanced model precision.

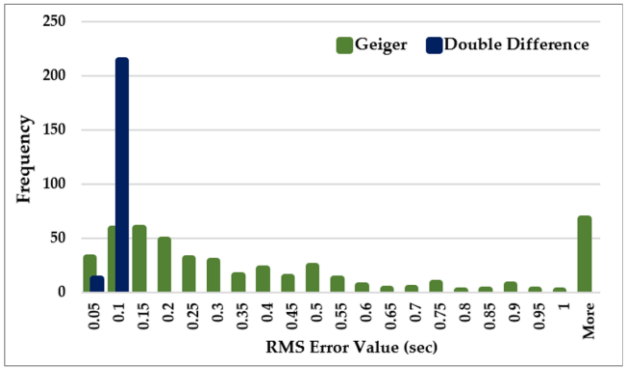

Figure 10 Histogram comparison of the RMS Error MEQ initial (Geiger) and final relocation (Double-Difference) values

This reduction indicates improved waveform coherence and stable inversion performance, consistent with findings by Zhang *et al*. (2021), who demonstrated that low RMS values reflect high inversion fidelity in microseismic applications. The distinct contrast between the scattered Geiger residuals and the compact HypoDD distribution underscores the method's effectiveness in minimizing travel-time discrepancies [47].

3.5 Hypocenter Distribution Maps

The spatial distribution of relocated micro-earthquake (MEQ) events (Figures 11-13) demonstrates the significant improvement achieved through the Double-Difference (HypoDD) relocation. Compared with the widely scattered Geiger solutions, the relocated epicenters exhibit a compact distribution concentrated along major fault zones, indicating enhanced positional accuracy and reduced uncertainty. The close alignment of seismic clusters with mapped faults and well zones suggests strong structural and hydrothermal control within the geothermal reservoir. Three-dimensional visualization confirms that most events are confined between -2.5 km and +0.5 km depth, coinciding with the active reservoir interval and reflecting fluid-induced fracture reactivation. Depth-frequency analysis further reveals that 94% of relocated events occur within -1.5 to +0.5 km, representing a substantial reduction in vertical dispersion. These findings are consistent with Chen *et al*. (2024), who noted that double-difference relocation enhances spatial coherence and mitigates velocity-model bias, resulting in improved correlation between seismicity and true fault geometries [37]. Collectively, the observed spatial compaction, fault alignment, and depth consistency validate the effectiveness of the HypoDD approach in producing high-fidelity representations of reservoir-scale microseismic activity.

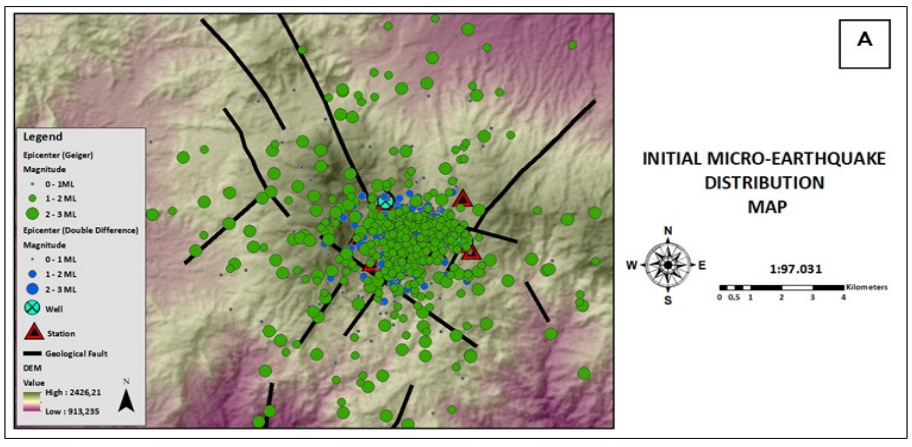

(a)

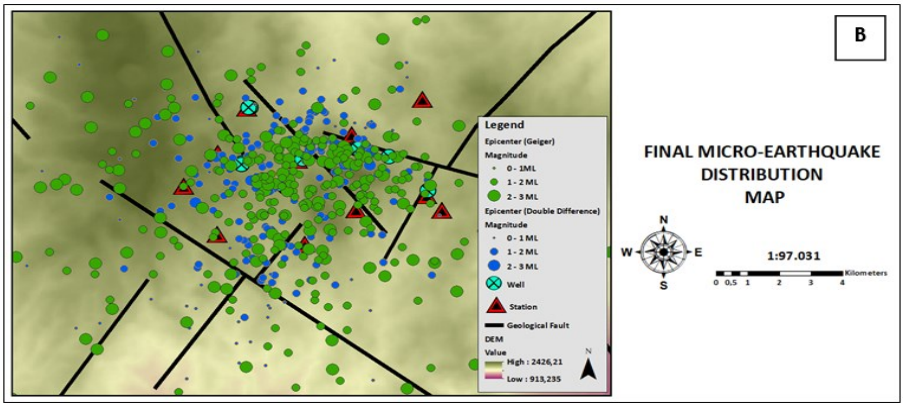

(b)

Figure 11 The comparison of initial MEQ epicenter location distribution using Geiger method (A) and the final MEQ epicenter location using Double-Difference method, involving a new 1D velocity model of the cluster region (B)

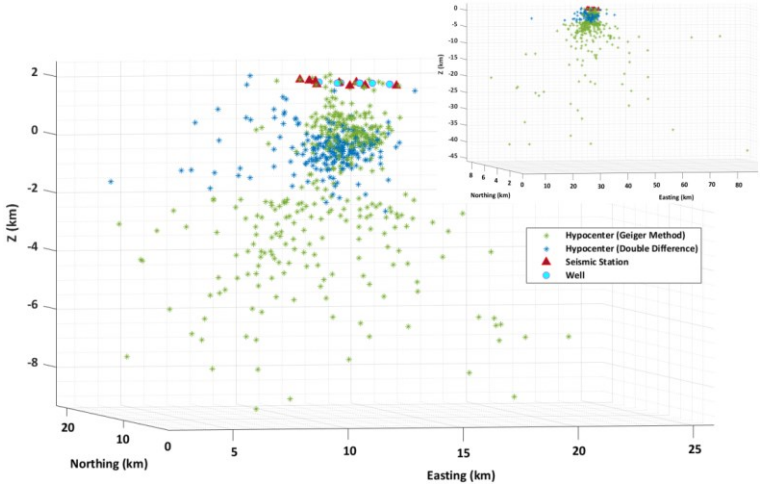

Figure 12 Comparison of the initial (green dots) and final (Double-Difference) (blue dots) MEQ depth distributions

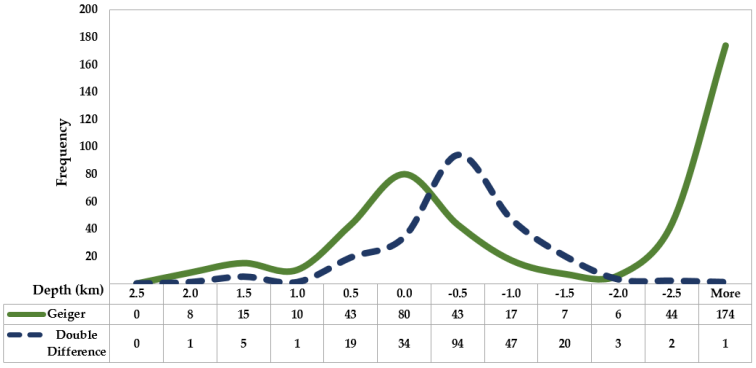

Depth (km)	2.5	2.0	1.5	1.0	0.5	0.0	-0.5	-1.0	-1.5	-2.0	-2.5	More
Geiger	0	8	15	10	43	80	43	17	7	6	44	174
Double Difference	0	1	5	1	19	34	94	47	20	3	2	1

Figure 13 Histogram comparison of RMS error values between Geiger and Double-Difference results

4.0 DISCUSSION

The integration of the refined 1D velocity model with the Double-Difference (HypoDD) relocation significantly enhanced the accuracy and consistency of micro-earthquake (MEQ) locations within the geothermal field. Coupled inversion effectively minimized travel-time misfits, reducing RMS residuals from 38.97 s in the initial Geiger results to an average of 0.07 s in the final solution, indicating strong model convergence and waveform coherence. The refined velocity structure, capturing the transition from low-velocity volcanic deposits to dense basement rocks, better represents subsurface heterogeneity and improves the precision of hypocentral depth estimates. The narrow RMS distribution (<0.1 s) confirms robust internal consistency between observed and synthetic arrivals, aligning with findings by Zhang *et al*. (2021) [47].

Spatially, the relocated events show distinct clustering along NW-SE fault traces and around injection–production wells, contrasting with the diffuse pattern from the Geiger solution. This alignment demonstrates that seismicity is dominantly controlled by fluid migration and fracture reactivation, with most events concentrated between -1.5 km and +0.5 km, corresponding to the active geothermal reservoir zone. The spatial correlation between seismicity, mapped structures, and geothermal infrastructure supports the interpretation of strong hydro-mechanical coupling driven by fluid-pressure changes, consistent with Chen *et al*. (2024) and Muttaqy *et al*. (2023) [25], [37]. These findings validate the effectiveness of the HypoDD method in delineating fracture-controlled permeability zones, similar to patterns reported in other Indonesian geothermal fields [12], [13]. While the current results provide a reliable high-resolution depiction of reservoir-scale seismicity, future integration of denser station networks and 3-D velocity inversions is recommended to further enhance structural imaging and fault delineation accuracy.

5.0 CONCLUSION

The integrated Coupled Velocity–Hypocenter inversion and Double-Difference (HypoDD) relocation significantly enhanced MEQ hypocenter accuracy, reducing RMS residuals from 38.97 s to 0.07 s and yielding a 93.66 % reduction in vertical deviation. About 94.3 % of events are confined between -1.5 km and +0.5 km, delineating the active geothermal reservoir zone. The relocated seismicity forms compact NW–SE clusters aligned with mapped faults and production–injection wells, indicating strong coupling between stress redistribution, fracture reactivation, and fluid flow. This refined methodological framework provides a reliable, replicable model for precise hypocenter determination, supporting early stress-change detection, improved induced-seismicity assessment, and safer geothermal reservoir management.

Acknowledgement

The authors would like to express their sincere gratitude to Institut Teknologi Sepuluh Nopember (ITS) for the continuous support, facilities, and academic environment that made this research possible. This study was conducted without any external funding or financial support.

Conflicts of Interest

The authors declare that there is no conflict of interest regarding the publication of this paper.

References

[1] Sharmin, T., N. R. Khan, M. S. Akram, and M. M. Ehsan. 2023. A State-of-the-Art Review on Geothermal Energy Extraction, Utilization, and Improvement Strategies: Conventional, Hybridized, and Enhanced Geothermal Systems. *International Journal of Thermofluids*. 18: 100323. https://doi.org/10.1016/j.ijft.2023.100323.

[2] Chappidi, S., A. Kumar, and J. Singh. 2024. Geothermal Energy Extraction Using a Novel Combined Coaxial and U-Shaped Closed-Loop System. *Geothermics*. 119: 102968. https://doi.org/10.1016/j.geothermics.2024.102968.

[3] Wu, Y., and P. Li. 2020. The Potential of Coupled Carbon Storage and Geothermal Extraction in a CO_2-Enhanced Geothermal System: A Review. *Geothermal Energy*. 8(1): 19. https://doi.org/10.1186/s40517-020-00173-w.

[4] Maurer, V., E. Gaucher, M. Grunberg, R. Koepke, R. Pestourie, and N. Cuenot. 2020. Seismicity Induced during the Development of the Rittershoffen Geothermal Field, France. *Geothermal Energy*. 8(1): 5. https://doi.org/10.1186/s40517-020-0155-2.

[5] Yaghoubi, A., M. Samaroo, and M. B. Dusseault. 2024. Anisotropic Behavior and Mechanical Characteristics of the Montney Formation. *International Journal of Rock Mechanics and Mining Sciences*. 180: 105831. https://doi.org/10.1016/j.ijrmms.2024.105831.

[6] Duda, M. I., A. Bakk, R. M. Holt, and J. F. Stenebråten. 2023. Anisotropic Poroelastic Modelling of Depletion-Induced Pore Pressure Changes in Valhall Overburden. *Rock Mechanics and Rock Engineering*. 56(4): 3115–3137. https://doi.org/10.1007/s00603-022-03192-0.

[7] Koray, A.-M., E. Gyimah, M. Metwally, H. Rahnema, and O. Tomomewo. 2025. Leveraging Machine Learning for Enhanced Reservoir Permeability Estimation in Geothermal Hotspots: A Case Study of the Williston Basin. *Geothermal Energy*. 13(1): 8. https://doi.org/10.1186/s40517-024-00323-4.

[8] Carbajal-Martínez, D., *et al*. 2024. Behavior of Amagmatic Orogenic Geothermal Systems: Insights from the Agua Blanca Fault, Baja California, Mexico. *Geochemistry, Geophysics, Geosystems*. 25(3): e2023GC011145. https://doi.org/10.1029/2023GC011145.

[9] Simanjuntak, A. V. H., K. H. Palgunadi, P. Supendi, D. Daryono, T. A. Prakoso, and U. Muksin. 2023. New Insight on the Active Fault System in the Halmahera Volcanic Arc, Indonesia, Derived from the 2022 Tobelo Earthquakes. *Seismological Research Letters*. 94(6): 2586–2594. https://doi.org/10.1785/0220230006.

[10] Utama, W., D. D. Warnana, and S. A. Garini. 2021. Identification of Micro-Earthquake Hypocenters Using Geiger and Coupled Velocity-Hypocenters Methods. *International Journal of Advanced Science, Engineering and Information Technology*. 11(1): 350–355. https://doi.org/10.18517/ijaseit.11.1.10589.

[11] Chen, Y., and L. Huang. 2019. Optimal Design of 3D Borehole Seismic Arrays for Microearthquake Monitoring in Anisotropic Media during Stimulations in the EGS Collab Project. *Geothermics*. 79: 61–66. https://doi.org/10.1016/j.geothermics.2019.01.009.

[12] Supendi, P., *et al*. 2022. The Kalaotoa Fault: A Newly Identified Fault that Generated the Mw 7.3 Flores Sea Earthquake. *The Seismic Record*. 2(3): 176–185. https://doi.org/10.1785/0320220015.

[13] Muksin, U., *et al*. 2023. Secondary Fault System in Northern Sumatra, Evidenced by Recent Seismicity and Geomorphic Structure. *Journal of Asian Earth Sciences*. 245: 105557. https://doi.org/10.1016/j.jseaes.2023.105557.

[14] McBrearty, I. W., and G. C. Beroza. 2025. Double Difference Earthquake Location with Graph Neural Networks. *Earth, Planets and Space*. 77(1): 127. https://doi.org/10.1186/s40623-025-02251-4.

[15] Soomro, R. A., S. Iqbal, M. A. Shah, and T. Iqbal. 2022. P-Wave Minimum 1D Velocity Model for Central and

Northern Pakistan. *Journal of Seismology*. 26(5): 1039–1049. https://doi.org/10.1007/s10950-022-10111-x.
[16] Krylov, A. A., *et al*. 2021. Ocean-Bottom Seismographs Based on Broadband MET Sensors: Architecture and Deployment Case Study in the Arctic. *Sensors*. 21(12). https://doi.org/10.3390/s21123979.
[17] Wang, K., W. Li, L. Zhao, D. Yu, and S. Wei. 2023. Research on Self-Noise Characteristics of Nine Types of Seismometers Obtained by PDF Representation Using Continuous Seismic Data from the Malingshan Seismic Station, China. *Sensors*. 23(1). https://doi.org/10.3390/s23010110.
[18] Daubar, I. J., *et al*. 2020. A New Crater Near InSight: Implications for Seismic Impact Detectability on Mars. *Journal of Geophysical Research: Planets*. 125(8): e2020JE006382. https://doi.org/10.1029/2020JE006382.
[19] Li, Y., B. J. Yang, J. Badal, X. P. Zhao, H. B. Lin, and R. L. Li. 2009. Chaotic System Detection of Weak Seismic Signals." *Geophysical Journal International*. 178(3): 1493–1522. https://doi.org/10.1111/j.1365-246X.2009.04232.x.
[20] Simanjuntak, A. V. H., and K. Ansari. 2023. Spatial Time Cluster Analysis and Earthquake Mechanism for Unknown Active Fault (Kalatoa Fault) in the Flores Sea. *Earth Science Informatics*. 16(3): 2649–2659. https://doi.org/10.1007/s12145-023-01067-8.
[21] Esquivel-Mendiola, L. I., M. Calò, A. Tramelli, and A. Figueroa-Soto. 2022. Optimization of Local Scale Seismic Networks Applied to Geothermal Fields: The Case of the Acoculco Caldera, Mexico. *Journal of South American Earth Sciences*. 119: 103995. https://doi.org/10.1016/j.jsames.2022.103995.
[22] Garini, S. A., Madlazim, and E. Rahmawati. 2014. Relokasi Hiposenter Gempa Bumi di Sulawesi Tengah dengan Menggunakan Metode Geiger dan Coupled Velocity-Hypocenter. *Jurnal Fisika*. 3(2): 107–112.
[23] Braszus, B., A. Rietbrock, C. Haberland, and T. Ryberg. 2024. AI Based 1-D P- and S-Wave Velocity Models for the Greater Alpine Region from Local Earthquake Data. *Geophysical Journal International*. 237(2): 916–930. https://doi.org/10.1093/gji/ggae077.
[24] Timsina, C., J. Mori, M. Yamada, and S. Ohmi. 2025. Improved 3D Velocity Model for Determining Aftershock Locations of the 2015 Gorkha, Nepal Earthquake. *Earth, Planets and Space*. 77(1): 132. https://doi.org/10.1186/s40623-025-02259-w.
[25] Muttaqy, F., *et al*. 2023. Double-Difference Earthquake Relocation Using Waveform Cross-Correlation in Central and East Java, Indonesia. *Geoscience Letters*. 10(1): 5. https://doi.org/10.1186/s40562-022-00259-2.
[26] Chakravarty, A., and S. Misra. 2023. Improved Hydraulic Fracture Characterization Using Representation Learning. *SPE EuropEC – Europe Energy Conference Featured at the 84th EAGE Annual Conference & Exhibition*. D031S010R002. https://doi.org/10.2118/214360-MS.
[27] Kang, M., Y. Huang, H. Xin, J. Song, X. Zhang, and R. Peng. 2023. Crustal Structures and Seismogenic Setting of the West Henan Region, North China, as Revealed by Magnetotelluric Imaging. *Pure and Applied Geophysics*. 180(11): 3835–3853. https://doi.org/10.1007/s00024-023-03369-w.
[28] Leong, Z. X., and T. Zhu. 2024. Machine Learning-Assisted Microearthquake Location Workflow for Monitoring the Newberry Enhanced Geothermal System. *Journal of Geophysical Research: Machine Learning and Computation*. 1(3): e2024JH000159. https://doi.org/10.1029/2024JH000159.
[29] Blanck, H., K. S. Vogfjörd, H. Geirsson, and V. Hjörleifsdóttir. 2022. Crustal Response to Inflation Imaged by Mapping of Subsurface Faults, Slip Directions, and Stress Changes during the 1993–1998 Unrest in Hengill, SW Iceland. *Journal of Volcanology and Geothermal Research*. 431: 107666. https://doi.org/10.1016/j.jvolgeores.2022.107666.
[30] Park, H., T.-S. Kang, H. J. Yoo, and D. Heo. 2023. Microearthquake Activity Associated with the 2016 ML 5.0 Offshore Ulsan Earthquake Sequence and Its Tectonic Implications. *Marine Geophysical Research*. 44(2): 9. https://doi.org/10.1007/s11001-023-09515-2.
[31] Pei, W., J. Zhuang, and S. Zhou. 2025. Stochastic Determination of Arrival Time and Initial Polarity of Seismic Waveform. *Earth, Planets and Space*. 77(1): 36. https://doi.org/10.1186/s40623-025-02161-5.
[32] Li, L., *et al*. 2020. Recent Advances and Challenges of Waveform-Based Seismic Location Methods at Multiple Scales. *Reviews of Geophysics*. 58(1): e2019RG000667. https://doi.org/10.1029/2019RG000667.
[33] Zheng, L., H. Yang, and G. Luo. 2025. Seismic Waveform Feature Extraction and Reservoir Prediction Based on CNN and UMAP: A Case Study of the Ordos Basin. *Applied Sciences*. 15(13). https://doi.org/10.3390/app15137377.
[34] Dahal, A., H. Tanyaş, and L. Lombardo. 2024. Full Seismic Waveform Analysis Combined with Transformer Neural Networks Improves Coseismic Landslide Prediction. *Communications Earth & Environment*. 5(1): 75. https://doi.org/10.1038/s43247-024-01243-8.
[35] Muksin, U., K. Bauer, and C. Haberland. 2013. Seismic Vp and Vp/Vs Structure of the Geothermal Area around Tarutung (North Sumatra, Indonesia) Derived from Local Earthquake Tomography. *Journal of Volcanology and Geothermal Research*. 260: 27–42. https://doi.org/10.1016/j.jvolgeores.2013.04.012.
[36] Afnimar, A., E. Yulianto, and R. Rasmid. 2015. Geological and Tectonic Implications Obtained from First Seismic Activity Investigation around Lembang Fault. *Geoscience Letters*. 2(1): 4. https://doi.org/10.1186/s40562-015-0020-5.
[37] Chen, H., S. Xue, and X. Zheng. 2024. Multi-Master Event Waveform Stacking Microseismic Location Method Based on Time-Frequency Transformation. *Journal of Applied Geophysics*. 220: 105267. https://doi.org/10.1016/j.jappgeo.2023.105267.
[38] Cheng, J., G. Song, X. Sun, L. Wen, and F. Li. 2018. Research Developments and Prospects on Microseismic Source Location in Mines. *Engineering*. 4(5): 653–660. https://doi.org/10.1016/j.eng.2018.08.004.
[39] Liao, Z., T. Feng, W. Yu, D. Cui, and G. Wu. 2022. Microseismic Source Location Method and Application Based on NM-PSO Algorithm. *Applied Sciences*. 12(17). https://doi.org/10.3390/app12178796.
[40] Wu, S., Y. Wang, Y. Zheng, and X. Chang. 2018. Microseismic Source Locations with Deconvolution Migration." *Geophysical Journal International*. 212(3): 2088–2115. https://doi.org/10.1093/gji/ggx518.
[41] Huang, G., J. Ba, Q. Du, and J. M. Carcione. 2019. Simultaneous Inversion for Velocity Model and Microseismic Sources in Layered Anisotropic Media. *Journal of Petroleum Science and Engineering*. 173: 1453–1463. https://doi.org/10.1016/j.petrol.2018.10.071.
[42] Okamoto, K., L. Yi, H. Asanuma, T. Okabe, Y. Abe, and M. Tsuzuki. 2018. Triggering Processes of Microseismic Events Associated with Water Injection in Okuaizu Geothermal Field, Japan. *Earth, Planets and Space*. 70(1): 15. https://doi.org/10.1186/s40623-018-0787-7.
[43] Ma, S., and D. W. Eaton. 2011. Combining Double-Difference Relocation with Regional Depth-Phase Modelling to Improve Hypocentre Accuracy. *Geophysical Journal International*. 185(2): 871–889. https://doi.org/10.1111/j.1365-246X.2011.04972.x.
[44] Lomax, A., and A. Michelini. 2009. Mwpd: A Duration–Amplitude Procedure for Rapid Determination of Earthquake Magnitude and Tsunamigenic Potential from P Waveforms. *Geophysical Journal International*. 176(1): 200–214. https://doi.org/10.1111/j.1365-246X.2008.03974.x.
[45] Lomax, A., and A. Savvaidis. 2022. High-Precision Earthquake Location Using Source-Specific Station Terms and Inter-Event Waveform Similarity. *Journal of Geophysical Research: Solid Earth*. 127(1): e2021JB023190. https://doi.org/10.1029/2021JB023190.
[46] Lomax, A., and A. Michelini. 2011. Tsunami Early Warning Using Earthquake Rupture Duration and P-Wave Dominant

Period: The Importance of Length and Depth of Faulting. *Geophysical Journal International*. 185(1): 283–291. https://doi.org/10.1111/j.1365-246X.2010.04916.x.

[47] Zhang, X., W. Zhang, and J. Zhang. 2021. Detecting and Locating Microseismic Events with Stacking Velocity Analysis for Surface Monitoring. *Journal of Applied Geophysics*. 195: 104470. https://doi.org/10.1016/j.jappgeo.2021.104470.

[48] Tian, X., J. Zhang, and W. Zhang. 2022. A Hybrid Workflow for Updating 1D Velocity Model and Microseismic Event Location. *Journal of Applied Geophysics*. 200: 104642. https://doi.org/10.1016/j.jappgeo.2022.104642.

[49] Katsumata, A., and T. Nishimiya. 2025. Three-Dimensional Velocity Structure Model for Hypocenter Determination in and around the Japanese Islands. *Earth, Planets and Space*. 77(1): 115. https://doi.org/10.1186/s40623-025-02243-4.